MOCVD growth of thick β -(Al)GaO films with fast growth rates

Lingyu Meng^{1,*}, A F M Anhar Uddin Bhuiyan¹, Dongsu Yu¹, Hsien-Lien Huang², Jinwoo

Hwang², and Hongping Zhao^{1,2,‡}

¹Department of Electrical and Computer Engineering, The Ohio State University, Columbus,

OH 43210. USA

²Department of Materials Science and Engineering, The Ohio State University, Columbus, OH

43210, USA

*Email: meng.480@osu.edu

‡Corresponding Author Email: zhao.2592@osu.edu

Abstract

In this work, we investigated the epitaxial growth of (010) β-Ga₂O₃ and β-(Al_xGa_{1-x})₂O₃ films using

metalorganic chemical vapor deposition (MOCVD) with trimethylgallium (TMGa) as the

precursor, aiming for high growth rates for thick films. We observed pyramid shaped defects in

the β-Ga₂O₃ epitaxial films, characterized by polygon-shaped bumps and inverted pyramids

embedded in the epi-films. To improve the surface morphology and suppress the defects formation,

we developed a novel approach that incorporates a small amount of aluminum (Al) during the

growth process. This addition led to significant improvements in surface morphology and

reductions in both the density and size of defects for the low-Al β-(Al_xGa_{1-x})₂O₃ films, with a

growth rate of 5.5 µm/h. Our findings demonstrate the effectiveness of this approach in optimizing

the surface morphology of thick β-(Al_xGa_{1-x})₂O₃ films with rapid growth rates. We achieved the

best surface for β-(Al_xGa_{1-x})₂O₃ in an 11 μm-thick film with approximately 2% Al composition,

grown at a rate of 5.5 µm/h. However, we also observed that defect density and size increase with

film thickness. Room temperature Hall measurements were used to characterize the electrical

properties of the low-Al β-(Al_xGa_{1-x})₂O₃ films, which revealed a decrease in Si incorporation

efficiency and room temperature mobility with increasing Al composition. Results indicated that

1

increasing the chamber pressure led to a decrease in both growth rate and Al composition at a constant [TMAl]/[TMGa + TMAl] molar flow rate ratio. The β -(Al_xGa_{1-x})₂O₃ films (~11 µm) with optimal surface quality were grown at chamber pressures between 60-100 torr. This work demonstrates the feasibility of growing (010) low-Al β -(Al_xGa_{1-x})₂O₃ thick films with high growth rates and minimal surface defects using MOCVD. Our findings provide valuable insights into β -(Al)GaO growth and suggest that introducing Al is an effective strategy for improving the surface morphology of β -(Al)GaO films. These results have important implications for the development of high-performance (Al)GaO based vertical power devices.

Keywords: Ultra-wide bandgap semiconductor, Ga₂O₃, AlGaO, MOCVD epitaxy, high growth rate, vertical power device, defects

I. Introduction

β-Ga₂O₃, an emerging semiconductor material, exhibits immense potential for high-power electronics attributed to its remarkable fundamental material properties, including an ultra-wide bandgap of 4.8 eV [1, 2] and a high critical field strength of 8 MV/cm [3]. The advancement of β-Ga₂O₃-based Schottky diodes and transistors has greatly expanded its promises for power device applications [4–20]. Moreover, the ability to control n-type doping within the range of 10¹⁶ cm⁻³ to 10²⁰ cm⁻³ [21–26], the successful epitaxial growth of semi-insulating layers [27, 28], and the availability of high-quality native substrates commercially [29] confer significant advantages to β-Ga₂O₃ for high-power device applications. Various methods have been employed to grow Ga₂O₃ on different oriented β-Ga₂O₃ substrates, such as molecular beam epitaxy (MBE) [8, 23, 30–36], pulsed laser deposition (PLD) [37–39], halide vapor phase epitaxy (HVPE) [22, 40–43], low-pressure chemical vapor deposition (LPCVD) [44–46], and metalorganic chemical vapor

deposition (MOCVD) [21, 24–26, 47–54]. In order to facilitate the application of high-performance power electronics with substantial breakdown capabilities, the incorporation of a thick drift layer becomes necessary. This layer effectively blocks higher reverse-biased voltage, resulting in a significantly enhanced breakdown voltage.

Thus far, homoepitaxial growth of β-Ga₂O₃ films with high growth rates (>10 μm/h) has been successfully achieved using HVPE [17, 55]. The availability of thick β-Ga₂O₃ homoepitaxial drift layers has facilitated the fabrication of various vertical β-Ga₂O₃ devices, including Schottky barrier diodes [17, 56, 57], p-n heterojunction diodes [58], and metal-insulator-semiconductor (MIS) diodes [59], on HVPE grown films. However, high-growth-rate HVPE processes often result in considerable surface roughness, characterized by surface steps and pits, necessitating the implementation of a chemical-mechanical polishing (CMP) process for surface preparation and device fabrication [42, 43]. Unfortunately, this additional step not only poses the risk of introducing impurities or contaminants onto the polished surface, but also makes it challenging to perform in-situ heterojunction growth. Among the various growth techniques for β-Ga₂O₃, MOCVD stands out as the most promising one due to its ability to produce high-quality crystalline thin films with high mobility and low compensation, which are crucial for realizing the theoretically predicted performance of β -Ga₂O₃ devices [24, 25, 52]. When triethylgallium (TEGa) is employed as the Ga precursor in MOCVD, the typical growth rate of β-Ga₂O₃ ranges from 0.2-1.0 μm/h [25, 50–52]. MOCVD-grown vertical β-Ga₂O₃ field plate Schottky barrier diodes have exhibited a low differential specific on-resistance of 0.67 mΩ·cm² and a breakdown electric field of 2.42 MV/cm [7]. However, the limited thickness of the drift layer (1.1 μm) poses a constraint on the breakdown voltage. Consequently, achieving a thick MOCVD β-Ga₂O₃ epi film with a fast growth rate becomes crucial. Previously, the use of trimethylgallium (TMGa) as a precursor for

MOCVD growth of β-Ga₂O₃ has demonstrated a room temperature mobility of 125 cm²/Vs with a carrier concentration of 1.5 x 10^{16} cm⁻³, and a low-temperature peak mobility of 23000 cm²/Vs at 32 K, indicating excellent material purity [53]. Recently, we have successfully employed TMGa as the Ga precursor for MOCVD, resulting in a high-quality epi-film with a growth rate of approximately 3 μm/h [26]. The carrier concentration can be controlled within the range of ~ 10^{16} to 10^{19} cm⁻³, and the room temperature mobility reaches up to 190 cm²/Vs with a carrier concentration of 1.8×10^{16} cm⁻³. Moreover, the extracted low compensation level is approximately 1.5×10^{15} cm⁻³. These findings indicate the great potential for developing vertical power device structures using MOCVD with TMGa. However, we have observed that the surface morphology becomes rougher with increasing film thickness and growth rate, potentially hindering its application in high power devices.

In this study, we conducted a comprehensive growth analysis to explore the growth parameters of MOCVD (010) thick β -Ga₂O₃ epi-films, utilizing TMGa as the Ga precursor. Here, we introduced a novel approach to improve the surface morphology of the thick β -Ga₂O₃ epi-films by incorporating a small quantity of Al. Our main objective is to advance the MOCVD growth technique for β -Ga₂O₃ aiming to achieve greater thickness and higher growth rates. Furthermore, alloying Ga₂O₃ with Al has the potential to increase the bandgap, leading to a higher breakdown field. These advancements have the potential to extend the possibilities for power device applications beyond the current limitations.

II. Experimental Section

MOCVD growths of (010) β-(Al_xGa_{1-x})₂O₃ films with thick thickness, fast growth rates, and low Al composition were grown on Fe-doped semi-insulating (010) β-Ga₂O₃ substrates (acquired from Novel Crystal Technology, Inc.). TMGa and Trimethylaluminum (TMAl) were used as the

Ga and Al precursors, respectively, pure oxygen (O₂) was used as the oxygen source, and Ar was used as the carrier gas. To introduce n-type doping, a diluted silane source with a concentration of 25 ppm was used as the Si precursor. The O₂ flow rate was set at 800 SCCM, and the growth temperature was maintained at 950 °C. The TMGa molar flow rate was adjusted in the range of 58 μmol/min to 87 μmol/min, resulting in growth rate varying from approximately 3-5.5 μm/h. Furthermore, the Al composition was controlled by modifying the [TMAl]/[TMGa + TMAl] molar flow rate ratio, ranging from 0% to 3.8%, in order to investigate its impact on surface morphology. From our previous extensive characterization of MOCVD grown (Al_xGa_{1-x})₂O₃ films with Al composition from low to high [60-62], we have demonstrated the uniform distribution of Al composition within the film especially for the cases with low-Al composition. The chamber pressure was adjusted between 40 and 100 Torr. Prior to the growth process, the substrate surface underwent thorough cleaning using acetone, isopropyl alcohol (IPA), and deionized water. For specific details regarding the growth parameters and corresponding film thicknesses, please refer to Table 1.

To determine the carrier concentrations and mobilities at room temperature, Hall measurements were performed using the Ecopia HMS-3000 Hall effect system with a magnetic field of 0.975 T. Ti/Au (30/100 nm) contacts were deposited on the four corners of the sample and annealed at 470°C under N₂ for 1 minute to form ohmic contacts. To analyze the surface morphologies, the field emission scanning electron microscopy (FESEM) (FEI Helios 600) was used. Cross-sectional FESEM images of the (Al_xGa_{1-x})₂O₃ films grown on co-loaded sapphire substrates were examined to estimate the film thicknesses and growth rates. Atomic force microscopy (AFM) using the Bruker AXS Dimension Icon was utilized to determine the surface roughness. The Al composition of the films was evaluated through X-ray diffraction (XRD)

measurements performed with a Bruker D8 Discover instrument, employing Cu Kα radiation with a wavelength of 1.5406 Å. For high-resolution STEM imaging, we utilized a Thermo Fisher Scientific Themis-Z scanning transmission electron microscope operating at 200 kV.

III. Results and Analysis

(010) β -(Al_xGa_{1-x})₂O₃ with a growth rate of 3 μ m/h with different Al compositions (0%-2.7%) were grown by tuning the TMGa/TMAl molar flow rate ratio (Sample #1-#4). The TMGa molar flow rate was kept as a constant at 58 μmol/min. The surface morphologies of these β-(Al_xGa₁x)2O3 films were characterized by FESEM images. Figures 1(a)-1(h) represent the FESEM images of low-Al β-(Al_xGa_{1-x})₂O₃ films grown with a growth rate of 3 μm/h with different Al compositions at x=0%, x=0.7%, 1.3%, and 2.7%, respectively. The characterized (Al_xGa_{1-x})₂O₃ films have a similar thickness of 3 µm. The observed surface defects on the various films have similar shapes. Note that these defects only appear when the film growth rate is relatively fast (e.g. 3 µm/h). Therefore, it is likely that the formation of these defects is associated with the high flow rate of TMGa precursor and thus high density of Ga adatoms on the growth surface. Due to the absence of energetically advantageous nucleation sites, the high-density Ga adatoms attach to neighboring Ga adatoms, initiating the formation of new islands and defects formation. From Fig. 1, as the Al composition increases from 0% to 2.7%, the density and size of the defects show monotonic decrease. It is believed that the incorporation of low Al during the MOCVD growth can facilitate the uniform nucleation of the adatoms and thus suppresses the defects formation. From our previous studies on the MOCVD growth of (100) (Al_xGa_{1-x})₂O₃ on (100) Ga₂O₃ substrates, the increase of Al precursor molar flow rate provides more uniform nucleation sites that suppresses the 2D island growth mode and thus improves the surface morphology [63]. The low-Al incorporation in MOCVD grown β-Ga₂O₃ with fast growth rate serves as a similar purpose. When

Al adatoms are supplied, considering its higher sticking coefficient than that of the Ga adatoms, this promotes more uniform nucleation of the (Al_xGa_{1-x})₂O₃ on the growth surface. Thus, incorporation of Al can facilitate (Al_xGa_{1-x})₂O₃ growth with surface morphologies.

Table 2 presents the electron concentration and room temperature (RT) mobility values for the samples grown at a growth rate of 3 μm/h with varying Al compositions. It is observed that the electron concentration decreases as the Al composition increases. This is attributed to the decrease of Si incorporation efficiency as the Al composition increase, which was confirmed from our previous studies [60]. Additionally, the RT mobility decreases with increasing Al composition, which can be attributed to higher impurity scattering associated with a higher Al composition.

To probe the structure of the surface defects observed in various samples, a series of characterizations are performed. Figure 2 shows the typical structure of the defect observed in the epitaxy film, characterized by a polygon-shaped bump and an inverted pyramid on the surface. The SEM and AFM images shown in Figure 2(a) and (b) indicate that the surface defect possesses a shorter axis aligned roughly along the [001] direction. Additionally, the cross-sectional STEM image in Figure 2(c) reveals the presence of an inverted pyramid structure within the epitaxial film. While there are similarities to the defects reported previously [54], there are also notable differences. In our study, the typical size of the defect appears larger, which can be attributed to the higher growth rate associated with a thicker film. Furthermore, we did not observe any nanotubes or dislocations from the substrate that were associated with the surface defects formation. From Figure 2(c), it can be observed that a 10%-Al AlGaO layer with a thickness of 70 nm was grown to identify the interface between the epi-film and substrate. The pyramid structure did not originate from the interface, indicating that the defect formed during the middle stages of

growth rather than from the initial stages. In contrast, Cooke et al. observed the apex of the pyramid and the nanotube meeting at the homoepitaxial film-substrate interface in their study [54].

Using high-angle annular dark-field (HAADF) imaging in scanning transmission electron microscopy (STEM), we investigated the atomic-scale details of the pyramid defects in the MOCVD grown films on (010) Ga₂O₃ substrate. By acquiring electron diffraction patterns, the crystallographic information along the projection was provided from both the substrate and the pyramid defect regions. Figure 3 shows an overview of the pyramid defect (Figure 3(a)), the atomic scale details within the interface regions (Figure 3(b)-3(d)), as well as the crystal planes identified by electron diffraction patterns (Figure 3(e)-3(g)). The magnified image shown in Figure 3(b) reveals distinct structural differences at the interface regions. The crystal structure outside of the defect region is oriented along the [001] direction, while the crystal structure within the pyramid defect is oriented along the $[1\overline{3}2]$ direction. In Figure 3(d), the crystal structure on the other side of the pyramid defect is oriented along $[\bar{1}3\bar{2}]$ direction, suggesting a two-fold crystal rotational symmetry of the pyramid defect structure along the (010) plane. The acquired diffraction patterns in Figures 3(e), 3(f), and 3(g) correspond to the crystal structures identified by STEM. This pyramid defect, distinct from previously characterized defects [64–67], has implications to the local properties during the growth of Ga₂O₃. Our STEM investigations reveal the absence of substrate-induced defects, in contrast to the recent study on surface defects [54]. From ref 54, the two crystal twins ($(\bar{4}10)$ and (410)) converge at an apex with an angle of 89° when viewed along the [001] zone axis of the film - which is consistent with our results. This suggests that the formation of pyramid defects is maybe driven by the preferred surface energy along the $(\bar{4}10)$ and (410) planes, resulting in termination of the epitaxial growth along the original [010] direction, rather than generating from the substrate.

In order to investigate the impact of Al-incorporation on the β-(Al)Ga₂O₃ MOCVD growth with even faster growth rates, we increased the TMGa molar flow rate to 87 μmol/min, resulting in a film growth rate of 5.5 μm/h. Figure 4(a) shows that the fast growth rate leads to a high density of pyramid defects and a rough surface morphology when the Al incorporation is 0%. As we increased the TMAl molar flow rate, the Al incorporation gradually increased from 0% to 1.7% (Fig. 4(b)), 2% (Fig. 4(c)), and 2.55% (Fig. 4(d)). The details of sample information for Sample #5 to Sample #8 can be found in Table 1. From Figure 4, it is evident that low-Al incorporation significantly improves the surface morphology of the samples grown at a similar growth rate (5.5 μm/h) and film thickness (5.5 μm). As the Al composition increases from 0% to 2.0%, the density of defects decreases while the typical size of the defects remains similar. However, the continuous increase in Al composition to 2.55% does not show any further improvement in surface morphology. Instead, the size of individual defects increases, as shown in Figure 4(d) and 4(h).

Table 2 lists the electron concentration and RT mobility for samples grown with different Al compositions at a growth rate of 5.5 μm/h (Sample #6-#8). The observed trend aligns with those observed in samples grown at a rate of 3 μm/h. Specifically, when keeping the silane flow rate constant, the electron Hall concentration decreases as the Al composition increases due to lower Si incorporation efficiency. Furthermore, the RT mobility decreases with increasing Al composition, as higher Al composition leads to increased impurity scattering.

To advance the application of β -(Al)Ga₂O₃ in vertical power devices, we performed MOCVD growth of films with varying Al compositions (ranging from 1.1% to 2.2%) and a thickness of 11 μ m at a growth rate of 5.5 μ m/h (Sample #9-#15), using a constant TMGa molar flow rate of 87 μ mol/min. Figure 5 shows the XRD ω -2 θ scan spectra of the β -(Al)Ga₂O₃ thin films, which were grown with various [TMAl]/[TMAl+TMGa] molar flow rate ratio ranging from 1.7% to 3.17%.

The XRD peaks at $2\theta = 60.9^{\circ}$ are from the β -Ga₂O₃ substrate, and the peaks from the β -(Al_xGa_{1-x})₂O₃ thin films exhibit a systematic shift towards higher 2θ angles as the Al composition increases. Note that the intensities of the β -(Al_xGa_{1-x})₂O₃ thin films maintain high due to the relatively low Al compositions and thus the high crystalline quality of the films. The FESEM images in Figures 6(a)–6(n) show the low-Al β -(Al_xGa_{1-x})₂O₃ films (11 μ m) grown with different Al compositions, including 0%, 1.1%, 1.3%, 1.7%, 1.9%, 2.1%, and 2.2%. As the Al composition increases from 0% to 1.9%, we observed a decrease in the density of defects while maintaining a similar defect size. However, further increasing the Al composition from 1.9% to 2.2% led to both an increase in the size and density of defects.

In this work, the effects of chamber pressure on the MOCVD β -(Al)Ga₂O₃ growth rates, Al composition, and surface morphology were further investigated. The total film thickness was maintained at approximately 11 µm (Sample #17-#19). As shown in Figures 7(a)-(h), the film growth rate decreases monotonically from 6.13 µm/h to 3 µm/h as the chamber pressure increases from 40 torr to 100 torr, which can be attributed to the enhanced gas-phase reactions of precursors at higher pressures. This observation agrees well with previous studies conducted on MOCVD growth of (010)-oriented β -Ga₂O₃ and β -(Al_xGa_{1-x})₂O₃ thin films using TEGa as the Ga precursor [25, 68]. Furthermore, we observed that as the chamber pressure increases, the Al incorporation decreases from 2.17% to 1.7% at a constant [TMAl]/[TMGa + TMAl] molar flow rate ratio, indicating low chamber pressure can facilitate Al incorporation efficiency. Form Fig. 7, the film surface morphology highly depends on the chamber pressure. The density and size of defects on β -(Al_xGa_{1-x})₂O₃ films (~11µm) decreases significantly at chamber pressures >= 60 torr. This reduction in defect density can be attributed to the lower density of the Ga adatoms due the enhanced gas phase reaction, which inhibits the formation of 3D islands. In addition, different

chamber pressure can also affect the adatom surface diffusion velocity and thus the nucleation process. Indeed, the study uncovered a trade-off between the growth rate and surface morphology of β -(Al_xGa_{1-x})₂O₃ films, which is influenced by the chamber pressure. Selecting the appropriate chamber pressure becomes crucial in achieving the desired balance between growth rate and surface quality in the MOCVD growth of β -(Al_xGa_{1-x})₂O₃ films. From this study, chamber pressure at 60 torr may be considered as an optimal growth pressure given its relatively high growth rate and comparatively low defect density.

Using the optimized growth conditions, a series of samples were grown with the same growth rate at 5.5 μ m/h and Al composition of ~2%, but with different growth duration of 1 hour, 2 hours and 3 hours. Figure 8 shows the FESEM and AFM images of the three films of low-Al β -(Al_xGa_{1-x})₂O₃ films (x~ 2%) with film thickness of 5.5 μ m, 11 μ m, and 16.5 μ m, respectively. It can be observed that as the film thickness increases, the size and density of defects also increase, indicating a correlation between film thickness and defect formation. Figures 8(d)-(f) show the corresponding AFM images of defect-free areas on the film surfaces. The root mean square (RMS) roughness values slightly increased from 1.27 nm to 2.51 nm with increasing film thickness, suggesting the potential for achieving thick β -(Al)Ga₂O₃ films suitable for power device applications, if the pyramid defects can be suppressed.

IV. Conclusions

In summary, a comprehensive investigation of the growth and surface morphology optimization of (010) β-Ga₂O₃ and low-Al β-(Al_xGa_{1-x})₂O₃ thick films using MOCVD was performed. The presence of pyramid-shaped defects in the epitaxial film was identified and characterized. The introduction of a small amount of aluminum was found to improve the surface morphology of the thick films. Optimized surface morphology with minimal defect density was

achieved in an 11 μ m-thick β -(Al_xGa_{1-x})₂O₃ film at a growth rate of 5.5 μ m/h and an Al composition of approximately 2%. However, it was observed that as the film thickness increased, the severity of surface defects also increased, indicating a tradeoff between film thickness and surface quality. Furthermore, the study demonstrated that higher chamber pressures during the MOCVD process led to reduced growth rates, but resulted in relatively smoother surface morphologies. These findings provide valuable insights into optimizing the surface morphology of (010) low-Al β -(Al_xGa_{1-x})₂O₃ thick films and have implications for the design and fabrication of high-power devices with improved performance.

Conflict of Interest Statement

On behalf of all authors, the corresponding author states that there is no conflict of interest.

Acknowledgement

The authors thank the financial support from the Air Force Office of Scientific Research FA9550-18-1-0479 (AFOSR, Dr. Ali Sayir), the NSF (Grant No. 2231026, No. 2019753), and the Semiconductor Research Corporation (SRC) under Task ID GRC 3007.001.

Data Availability

The data that support the findings of this study are available from the corresponding author upon reasonable request.

Reference

(1) Tippins, H. H. Optical Absorption and Photoconductivity in the Band Edge of β -Ga₂O₃. *Phys. Rev.* **1965**, *140*, A316–A319.

- (2) Onuma, T.; Fujioka, S.; Yamaguchi, T.; Higashiwaki, M.; Sasaki, K.; Masui, T.; Honda, T. Correlation between Blue Luminescence Intensity and Resistivity in β-Ga₂O₃ Single Crystals. *Appl. Phys. Lett.* **2013**, *103*, 041910.
- (3) Higashiwaki, M.; Sasaki, K.; Kuramata, A.; Masui, T.; Yamakoshi, S. Gallium Oxide (Ga₂O₃) Metal-Semiconductor Field-Effect Transistors on Single-Crystal β-Ga₂O₃ (010) Substrates. *Appl. Phys. Lett.* **2012**, *100*, 013504.
- (4) Farzana, E.; Zhang, Z.; Paul, P. K.; Arehart, A. R.; Ringel, S. A. Influence of Metal Choice on (010) β-Ga₂O₃ Schottky Diode Properties. *Appl. Phys. Lett.* **2017**, *110*, 202102.
- (5) Farzana, E.; Ahmadi, E.; Speck, J. S.; Arehart, A. R.; Ringel, S. A. Deep Level Defects in Ge-Doped (010) β-Ga₂O₃ Layers Grown by Plasma-Assisted Molecular Beam Epitaxy. *J. Appl. Phys.* **2018**, *123*, 161410.
- (6) Farzana, E.; Mauze, A.; Varley, J. B.; Blue, T. E.; Speck, J. S.; Arehart, A. R.; Ringel, S. A. Influence of Neutron Irradiation on Deep Levels in Ge-Doped (010) β-Ga₂O₃ Layers Grown by Plasma-Assisted Molecular Beam Epitaxy. *APL Mater.* **2019**, *7*, 121102.
- (7) Farzana, E.; Alema, F.; Ho, W. Y.; Mauze, A.; Itoh, T.; Osinsky, A.; Speck, J. S. Vertical β-Ga₂O₃ Field Plate Schottky Barrier Diode from Metal-Organic Chemical Vapor Deposition. *Appl. Phys. Lett.* **2021**, *118*, 162109.
- (8) Sasaki, K.; Higashiwaki, M.; Kuramata, A.; Masui, T.; Yamakoshi, S. MBE Grown Ga₂O₃ and Its Power Device Applications. *J. Cryst. Growth* **2013**, *378*, 591–595.
- (9) Sasaki, K.; Kuramata, A.; Masui, T.; Víllora, E. G.; Shimamura, K.; Yamakoshi, S. Device-Quality β-Ga₂O₃ Epitaxial Films Fabricated by Ozone Molecular Beam Epitaxy. *Appl. Phys. Express* **2012**, *5*, 035502.
- (10) Allen, N.; Xiao, M.; Yan, X.; Sasaki, K.; Tadjer, M. J.; Ma, J.; Zhang, R.; Wang, H.; Zhang, Y. Vertical Ga₂O₃ Schottky Barrier Diodes With Small-Angle Beveled Field Plates: A Baliga's Figure-of-Merit of 0.6 GW/cm². *IEEE Electron Device Lett.* **2019**, *40*, 1399–1402.
- (11) Joishi, C.; Rafique, S.; Xia, Z.; Han, L.; Krishnamoorthy, S.; Zhang, Y.; Lodha, S.; Zhao, H.; Rajan, S. Low-Pressure CVD-Grown β -Ga₂O₃ Bevel-Field-Plated Schottky Barrier Diodes. *Appl. Phys. Express* **2018**, *11*, 031101.
- (12) Saha, S.; Meng, L.; Feng, Z.; Bhuiyan, A F M A. U.; Zhao, H.; Singisetti, U. Schottky Diode Characteristics on High-Growth Rate LPCVD β-Ga₂O₃ Films on (010) and (001) Ga₂O₃ Substrates. *Appl. Phys. Lett.* **2022**, *120*, 122106.
- (13) Yang, J.; Ahn, S.; Ren, F.; Pearton, S. J.; Jang, S.; Kuramata, A. High Breakdown Voltage (201) β-Ga₂O₃ Schottky Rectifiers. *IEEE Electron Device Lett.* **2017**, *38* (7), 906–909.
- (14) Yang, J.; Ren, F.; Tadjer, M.; Pearton, S. J.; Kuramata, A. 2300V Reverse Breakdown Voltage Ga₂O₃ Schottky Rectifiers. *ECS J. Solid State Sci. Technol.* **2018**, *7*, Q92.
- (15) Carey, P. H.; Yang, J.; Ren, F.; Sharma, R.; Law, M.; Pearton, S. J. Comparison of Dual-Stack Dielectric Field Plates on β-Ga₂O₃ Schottky Rectifiers. *ECS J. Solid State Sci. Technol.* **2019**, *8*, Q3221.
- (16) Jian, Z. (Ashley); Mohanty, S.; Ahmadi, E. Temperature-Dependent Current-Voltage Characteristics of β-Ga₂O₃ Trench Schottky Barrier Diodes. *Appl. Phys. Lett.* **2020**, *116*, 152104.
- (17) Li, W.; Nomoto, K.; Hu, Z.; Jena, D.; Xing, H. G. Field-Plated Ga_2O_3 Trench Schottky Barrier Diodes With a $BV^2/R_{on,sp}$ of up to 0.95 GW/cm^2 . *IEEE Electron Device Lett.* **2020**, 41, 107–110.
- (18) Li, W.; Hu, Z.; Nomoto, K.; Zhang, Z.; Hsu, J.-Y.; Thieu, Q. T.; Sasaki, K.; Kuramata, A.; Jena, D.; Xing, H. G. 1230 V β -Ga₂O₃ Trench Schottky Barrier Diodes with an Ultra-Low Leakage Current of <1 μ A/cm². *Appl. Phys. Lett.* **2018**, *113*, 202101.

- (19) Lin, C.-H.; Yuda, Y.; Wong, M. H.; Sato, M.; Takekawa, N.; Konishi, K.; Watahiki, T.; Yamamuka, M.; Murakami, H.; Kumagai, Y.; Higashiwaki, M. Vertical Ga₂O₃ Schottky Barrier Diodes With Guard Ring Formed by Nitrogen-Ion Implantation. *IEEE Electron Device Lett.* **2019**, *40*, 1487–1490.
- (20) Wong, M. H.; Goto, K.; Murakami, H.; Kumagai, Y.; Higashiwaki, M. Current Aperture Vertical β-Ga₂O₃ MOSFETs Fabricated by N- and Si-Ion Implantation Doping. *IEEE Electron Device Lett.* **2019**, *40*, 431–434.
- (21) Baldini, M.; Albrecht, M.; Fiedler, A.; Irmscher, K.; Klimm, D.; Schewski, R.; Wagner, G. Semiconducting Sn-Doped β-Ga₂O₃ Homoepitaxial Layers Grown by Metal Organic Vapour-Phase Epitaxy. *J. Mater. Sci.* **2016**, *51*, 3650–3656.
- (22) Goto, K.; Konishi, K.; Murakami, H.; Kumagai, Y.; Monemar, B.; Higashiwaki, M.; Kuramata, A.; Yamakoshi, S. Halide Vapor Phase Epitaxy of Si Doped β -Ga₂O₃ and Its Electrical Properties. *Thin Solid Films* **2018**, *666*, 182–184.
- (23) Ahmadi, E.; Koksaldi, O. S.; Kaun, S. W.; Oshima, Y.; Short, D. B.; Mishra, U. K.; Speck, J. S. Ge Doping of β-Ga₂O₃ Films Grown by Plasma-Assisted Molecular Beam Epitaxy. *Appl. Phys. Express* **2017**, *10*, 041102.
- (24) Zhang, Y.; Alema, F.; Mauze, A.; Koksaldi, O. S.; Miller, R.; Osinsky, A.; Speck, J. S. MOCVD Grown Epitaxial β -Ga₂O₃ Thin Film with an Electron Mobility of 176 cm²/V s at Room Temperature. *APL Mater.* **2019**, *7*, 022506.
- (25) Feng, Z.; Bhuiyan, A F M A. U.; Karim, M. R.; Zhao, H. MOCVD Homoepitaxy of Si-Doped (010) β-Ga₂O₃ Thin Films with Superior Transport Properties. *Appl. Phys. Lett.* **2019**, *114*, 250601.
- (26) Meng, L.; Feng, Z.; Bhuiyan, A F M A. U.; Zhao, H. High-Mobility MOCVD β-Ga₂O₃ Epitaxy with Fast Growth Rate Using Trimethylgallium. *Cryst. Growth Des.* **2022**, *22*, 3896–3904.
- (27) Feng, Z.; Bhuiyan, A F M A. U.; Kalarickal, N. K.; Rajan, S.; Zhao, H. Mg Acceptor Doping in MOCVD (010) β-Ga₂O₃. *Appl. Phys. Lett.* **2020**, *117*, 222106.
- (28) Mauze, A.; Zhang, Y.; Itoh, T.; Mates, T. E.; Peelaers, H.; Van de Walle, C. G.; Speck, J. S. Mg Doping and Diffusion in (010) β-Ga₂O₃ Films Grown by Plasma-Assisted Molecular Beam Epitaxy. *J. Appl. Phys.* **2021**, *130*, 235301.
- (29) Kuramata, A.; Koshi, K.; Watanabe, S.; Yamaoka, Y.; Masui, T.; Yamakoshi, S. High-Quality β-Ga₂O₃ Single Crystals Grown by Edge-Defined Film-Fed Growth. *Jpn. J. Appl. Phys.* **2016**, *55*, 1202A2.
- (30) Tsai, M.-Y.; Bierwagen, O.; White, M. E.; Speck, J. S. β-Ga₂O₃ Growth by Plasma-Assisted Molecular Beam Epitaxy. *J. Vac. Sci. Technol. A* **2010**, *28*, 354–359.
- (31) Vogt, P.; Bierwagen, O. Reaction Kinetics and Growth Window for Plasma-Assisted Molecular Beam Epitaxy of Ga₂O₃: Incorporation of Ga vs. Ga₂O Desorption. *Appl. Phys. Lett.* **2016**, *108*, 072101.
- (32) Vogt, P.; Brandt, O.; Riechert, H.; Lähnemann, J.; Bierwagen, O. Metal-Exchange Catalysis in the Growth of Sesquioxides: Towards Heterostructures of Transparent Oxide Semiconductors. *Phys. Rev. Lett.* **2017**, *119*, 196001.
- (33) Vogt, P.; Mauze, A.; Wu, F.; Bonef, B.; Speck, J. S. Metal-Oxide Catalyzed Epitaxy (MOCATAXY): The Example of the O Plasma-Assisted Molecular Beam Epitaxy of β-(Al_xGa_{1-x})₂O₃/β-Ga₂O₃ Heterostructures. *Appl. Phys. Express* **2018**, *11*, 115503.
- (34) Vogt, P.; Hensling, F. V. E.; Azizie, K.; Chang, C. S.; Turner, D.; Park, J.; McCandless, J. P.; Paik, H.; Bocklund, B. J.; Hoffman, G.; Bierwagen, O.; Jena, D.; Xing, H. G.; Mou, S.;

- Muller, D. A.; Shang, S.-L.; Liu, Z.-K.; Schlom, D. G. Adsorption-Controlled Growth of Ga₂O₃ by Suboxide Molecular-Beam Epitaxy. *APL Mater.* **2021**, *9*, 031101.
- (35) Mauze, A.; Zhang, Y.; Itoh, T.; Wu, F.; Speck, J. S. Metal Oxide Catalyzed Epitaxy (MOCATAXY) of β-Ga₂O₃ Films in Various Orientations Grown by Plasma-Assisted Molecular Beam Epitaxy. *APL Mater.* **2020**, *8*, 021104.
- (36) Mazzolini, P.; Falkenstein, A.; Wouters, C.; Schewski, R.; Markurt, T.; Galazka, Z.; Martin, M.; Albrecht, M.; Bierwagen, O. Substrate-Orientation Dependence of β-Ga₂O₃ (100), (010), (001), and ($\bar{2}01$) Homoepitaxy by Indium-Mediated Metal-Exchange Catalyzed Molecular Beam Epitaxy (MEXCAT-MBE). *APL Mater.* **2020**, *8*, 011107.
- (37) Orita, M.; Hiramatsu, H.; Ohta, H.; Hirano, M.; Hosono, H. Preparation of Highly Conductive, Deep Ultraviolet Transparent β -Ga₂O₃ Thin Film at Low Deposition Temperatures. *Thin Solid Films* **2002**, *411*, 134–139.
- (38) Leedy, K. D.; Chabak, K. D.; Vasilyev, V.; Look, D. C.; Boeckl, J. J.; Brown, J. L.; Tetlak, S. E.; Green, A. J.; Moser, N. A.; Crespo, A.; Thomson, D. B.; Fitch, R. C.; McCandless, J. P.; Jessen, G. H. Highly Conductive Homoepitaxial Si-Doped Ga₂O₃ Films on (010) β-Ga₂O₃ by Pulsed Laser Deposition. *Appl. Phys. Lett.* **2017**, *111*, 012103.
- (39) Matsuzaki, K.; Hiramatsu, H.; Nomura, K.; Yanagi, H.; Kamiya, T.; Hirano, M.; Hosono, H. Growth, Structure and Carrier Transport Properties of Ga₂O₃ Epitaxial Film Examined for Transparent Field-Effect Transistor. *Thin Solid Films* **2006**, *496*, 37–41.
- (40) Nomura, K.; Goto, K.; Togashi, R.; Murakami, H.; Kumagai, Y.; Kuramata, A.; Yamakoshi, S.; Koukitu, A. Thermodynamic Study of β-Ga₂O₃ Growth by Halide Vapor Phase Epitaxy. *J. Cryst. Growth* **2014**, *405*, 19–22.
- (41) Oshima, Y.; Villora, E. G.; Shimamura, K. Halide Vapor Phase Epitaxy of Twin-Free α-Ga₂O₃ on Sapphire (0001) Substrates. *Appl. Phys. Express* **2015**, *8*, 055501.
- (42) Murakami, H.; Nomura, K.; Goto, K.; Sasaki, K.; Kawara, K.; Thieu, Q. T.; Togashi, R.; Kumagai, Y.; Higashiwaki, M.; Kuramata, A.; Yamakoshi, S.; Monemar, B.; Koukitu, A. Homoepitaxial Growth of β-Ga₂O₃ Layers by Halide Vapor Phase Epitaxy. *Appl. Phys. Express* **2014**, *8*, 015503.
- (43) Leach, J. H.; Udwary, K.; Rumsey, J.; Dodson, G.; Splawn, H.; Evans, K. R. Halide Vapor Phase Epitaxial Growth of β-Ga₂O₃ and α-Ga₂O₃ Films. *APL Mater.* **2019**, *7*, 022504.
- (44) Rafique, S.; Karim, M. R.; Johnson, J. M.; Hwang, J.; Zhao, H. LPCVD Homoepitaxy of Si Doped β-Ga₂O₃ Thin Films on (010) and (001) Substrates. *Appl. Phys. Lett.* **2018**, *112*, 052104.
- (45) Rafique, S.; Han, L.; Neal, A. T.; Mou, S.; Boeckl, J.; Zhao, H. Towards High-Mobility Heteroepitaxial β-Ga₂O₃ on Sapphire Dependence on The Substrate Off-Axis Angle. *Phys. Status Solidi A* **2018**, *215*, 1700467.
- (46) Zhang, Y.; Feng, Z.; Karim, M. R.; Zhao, H. High-Temperature Low-Pressure Chemical Vapor Deposition of β-Ga₂O₃. *J. Vac. Sci. Technol. A* **2020**, *38*, 050806.
- (47) Baldini, M.; Albrecht, M.; Fiedler, A.; Irmscher, K.; Schewski, R.; Wagner, G. Editors' Choice—Si- and Sn-Doped Homoepitaxial β-Ga₂O₃ Layers Grown by MOVPE on (010)-Oriented Substrates. *ECS J. Solid State Sci. Technol.* **2016**, *6*, Q3040.
- (48) Wagner, G.; Baldini, M.; Gogova, D.; Schmidbauer, M.; Schewski, R.; Albrecht, M.; Galazka, Z.; Klimm, D.; Fornari, R. Homoepitaxial Growth of β-Ga₂O₃ Layers by Metal-Organic Vapor Phase Epitaxy. *Phys. Status Solidi A* **2014**, *211*, 27–33.
- (49) Fiedler, A.; Schewski, R.; Baldini, M.; Galazka, Z.; Wagner, G.; Albrecht, M.; Irmscher, K. Influence of Incoherent Twin Boundaries on the Electrical Properties of β-Ga₂O₃ Layers

- Homoepitaxially Grown by Metal-Organic Vapor Phase Epitaxy. J. Appl. Phys. 2017, 122, 165701.
- (50) Schewski, R.; Lion, K.; Fiedler, A.; Wouters, C.; Popp, A.; Levchenko, S. V.; Schulz, T.; Schmidbauer, M.; Bin Anooz, S.; Grüneberg, R.; Galazka, Z.; Wagner, G.; Irmscher, K.; Scheffler, M.; Draxl, C.; Albrecht, M. Step-Flow Growth in Homoepitaxy of β-Ga₂O₃ (100)—The Influence of the Miscut Direction and Faceting. *APL Mater.* **2019**, *7*, 022515.
- (51) Bin Anooz, S.; Grüneberg, R.; Wouters, C.; Schewski, R.; Albrecht, M.; Fiedler, A.; Irmscher, K.; Galazka, Z.; Miller, W.; Wagner, G.; Schwarzkopf, J.; Popp, A. Step Flow Growth of β-Ga₂O₃ Thin Films on Vicinal (100) β-Ga₂O₃ Substrates Grown by MOVPE. *Appl. Phys. Lett.* **2020**, *116*, 182106.
- (52) Feng, Z.; Bhuiyan, A F M A. U.; Xia, Z.; Moore, W.; Chen, Z.; McGlone, J. F.; Daughton, D. R.; Arehart, A. R.; Ringel, S. A.; Rajan, S.; Zhao, H. Probing Charge Transport and Background Doping in Metal-Organic Chemical Vapor Deposition-Grown (010) β-Ga₂O₃. *Phys. Status Solidi RRL Rapid Res. Lett.* **2020**, *14*, 2000145.
- (53) Seryogin, G.; Alema, F.; Valente, N.; Fu, H.; Steinbrunner, E.; Neal, A. T.; Mou, S.; Fine, A.; Osinsky, A. MOCVD Growth of High Purity Ga₂O₃ Epitaxial Films Using Trimethylgallium Precursor. *Appl. Phys. Lett.* **2020**, *117*, 262101.
- (54) Cooke, J.; Ranga, P.; Bhattacharyya, A.; Cheng, X.; Wang, Y.; Krishnamoorthy, S.; Scarpulla, M. A.; Sensale-Rodriguez, B. Sympetalous Defects in Metalorganic Vapor Phase Epitaxy (MOVPE)-Grown Homoepitaxial β-Ga₂O₃ Films. *J. Vac. Sci. Technol. A* **2023**, *41*, 013406.
- (55) Hu, Z.; Nomoto, K.; Li, W.; Tanen, N.; Sasaki, K.; Kuramata, A.; Nakamura, T.; Jena, D.; Xing, H. G. Enhancement-Mode Ga₂O₃ Vertical Transistors With Breakdown Voltage >1 KV. *IEEE Electron Device Lett.* **2018**, *39*, 869–872.
- (56) Konishi, K.; Goto, K.; Murakami, H.; Kumagai, Y.; Kuramata, A.; Yamakoshi, S.; Higashiwaki, M. 1-kV Vertical Ga₂O₃ Field-Plated Schottky Barrier Diodes. *Appl. Phys. Lett.* **2017**, *110*, 103506.
- (57) Sasaki, K.; Wakimoto, D.; Thieu, Q. T.; Koishikawa, Y.; Kuramata, A.; Higashiwaki, M.; Yamakoshi, S. First Demonstration of Ga₂O₃ Trench MOS-Type Schottky Barrier Diodes. *IEEE Electron Device Lett.* **2017**, *38*, 783–785.
- (58) Yan, Q.; Gong, H.; Zhang, J.; Ye, J.; Zhou, H.; Liu, Z.; Xu, S.; Wang, C.; Hu, Z.; Feng, Q.; Ning, J.; Zhang, C.; Ma, P.; Zhang, R.; Hao, Y. β-Ga₂O₃ Hetero-Junction Barrier Schottky Diode with Reverse Leakage Current Modulation and BV²/R_{on,Sp} Value of 0.93 GW/cm². *Appl. Phys. Lett.* **2021**, *118*, 122102.
- (59) Li, W.; Nomoto, K.; Hu, Z.; Tanen, N.; Sasaki, K.; Kuramata, A.; Jena, D.; Xing, H. G. 1.5 KV Vertical Ga₂O₃ Trench-MIS Schottky Barrier Diodes. In *2018 76th Device Research Conference (DRC)*; 2018; pp 1–2.
- (60) Bhuiyan, A F M A. U.; Feng, Z.; Meng, L.; Fiedler, A.; Huang, H.-L.; Neal, A. T.; Steinbrunner, E.; Mou, S.; Hwang, J.; Rajan, S.; Zhao, H. Si Doping in MOCVD Grown (010) β-(Al_xGa_{1-x})₂O₃ Thin Films. *Journal of Applied Physics* **2022**, *131*, 145301.
- (61) Bhuiyan, A F M A. U.; Meng, L.; Huang, H.-L.; Hwang, J.; Zhao, H. In Situ MOCVD Growth and Band Offsets of Al2O3 Dielectric on β- Ga₂O₃ and β-(Al_xGa_{1-x})₂O₃ Thin Films. *Journal of Applied Physics* **2022**, *132*, 165301.
- (62) Bhuiyan, A F M A. U.; Feng, Z.; Johnson, J. M.; Huang, H.-L.; Sarker, J.; Zhu, M.; Karim, M. R.; Mazumder, B.; Hwang, J.; Zhao, H. Phase Transformation in MOCVD Growth of β -(Al_xGa_{1-x})₂O₃ Thin Films. *APL Materials* **2020**, *8*, 031104.

- (63) Bhuiyan, A F M A. U.; Feng, Z.; Johnson, J. M.; Huang, H.-L.; Hwang, J.; Zhao, H. MOCVD Epitaxy of Ultrawide Bandgap β-(Al_xGa_{1-x})₂O₃ with High-Al Composition on (100) β-Ga₂O₃ Substrates. *Cryst. Growth Des.* **2020**, *20*, 6722–6730.
- (64) Nakai, K.; Nagai, T.; Noami, K.; Futagi, T. Characterization of Defects in β-Ga₂O₃ Single Crystals. *Jpn. J. Appl. Phys.* **2015**, *54*, 051103.
- (65) Kasu, M.; Hanada, K.; Moribayashi, T.; Hashiguchi, A.; Oshima, T.; Oishi, T.; Koshi, K.; Sasaki, K.; Kuramata, A.; Ueda, O. Relationship between Crystal Defects and Leakage Current in β-Ga₂O₃ Schottky Barrier Diodes. *Jpn. J. Appl. Phys.* **2016**, *55*, 1202BB.
- (66) Ueda, O.; Ikenaga, N.; Koshi, K.; Iizuka, K.; Kuramata, A.; Hanada, K.; Moribayashi, T.; Yamakoshi, S.; Kasu, M. Structural Evaluation of Defects in β-Ga₂O₃ Single Crystals Grown by Edge-Defined Film-Fed Growth Process. *Jpn. J. Appl. Phys.* **2016**, *55*, 1202BD.
- (67) Sdoeung, S.; Sasaki, K.; Kawasaki, K.; Hirabayashi, J.; Kuramata, A.; Kasu, M. Polycrystalline Defects—Origin of Leakage Current—in Halide Vapor Phase Epitaxial (001) β-Ga₂O₃ Schottky Barrier Diodes Identified via Ultrahigh Sensitive Emission Microscopy and Synchrotron X-Ray Topography. *Appl. Phys. Express* **2021**, *14*, 036502.
- (68) Bhuiyan, A F M A. U.; Feng, Z.; Meng, L.; Zhao, H. MOCVD Growth of (010) β -(Al_xGa_{1-x})₂O₃ Thin Films. *J. Mater. Res.* **2021**, *36*, 4804–4815.

Table Caption

Table 1. Summary of (010) low-Al β -(Al_xGa_{1-x})₂O₃ films grown with different growth conditions: TMGa molar flow rate (58-87 μmol/min), [TMAl]/[TMGa + TMAl] molar flow rate ratio (0-3.8%), growth duration (1-3 hours), and chamber pressure (40–100 Torr).

Table 2. Room temperature Hall mobility and electron concentration for (010) low-Al β- $(Al_xGa_{1-x})_2O_3$ films with various Al compositions grown with different growth rates.

Figure Captions

- **Fig 1**. Surface view FESEM images of low-Al β-(Al_xGa_{1-x})₂O₃ films (~3 μm) grown with a growth rate of 3 μm/h with (a) x=0% (#1), (b) x=0.7% (#2), (c) x=1.3% (#3), (d) x=2.7% (#4). The corresponding high magnification images are shown in (e)-(h).
- **Fig 2**. Pyramid-shaped defect consisting of bump on the surface with a polygon shape and inverted pyramid in the epitaxy film. (a) AFM image, (b) Surface view FESEM image, and (c) HAADF-STEM image.
- Fig 3. (a) High resolution STEM images of the interface between the pyramid defect and the MOCVD grown film on (010) β -Ga₂O₃ substrate: (b) left side (c) bottom, and (d) right side. Diffraction patterns reveal the identified crystal structures for [001], [1 $\overline{3}$ 2], and [$\overline{1}$ 3 $\overline{2}$] at the (e) substrate (f) left side (g) right side of pyramid defect, respectively.
- **Fig 4**. Surface view FESEM images of low-Al β-(Al_xGa_{1-x})₂O₃ films (~5.5 μm) grown with a growth rate of 5.5 μm/h with (a) x=0% (#5), (b) x=1.7% (#6), (c) x=2% (#7), (d) x=2.55% (#8). The corresponding high magnification images are shown in (e)-(h).
- Fig 5: XRD ω -2θ scan profiles of low-Al β -(Al_xGa_{1-x})₂O₃ films grown on (010) β -Ga₂O₃ substrates with various Al compositions. The extracted Al compositions were 1.1%, 1.3%, 1.7%, 1.9%, 2.1%, and 2.2%.
- Fig 6. Surface view FESEM images of low-Al β-(Al_xGa_{1-x})₂O₃ films (~11 μm) grown with a growth rate of 5.5μm/h with (a) x=0% (#15) (b) x=1.1% (#14), (c) x=1.3% (#13), (d) x=1.7% (#12), (e) x=1.9% (#11), (f) x=2.1% (#10), (g) x=2.2% (#9). The corresponding high magnification images are shown in (h)-(n).

Fig 7. Surface view FESEM images of low-Al β-(Al_xGa_{1-x})₂O₃ films (~11 μm) grown at different chamber pressure: (a) 40 torr x=2.17% (#19), (b) 60 torr x=1.9% (#11), (c) 80 torr x=1.8% (#18), and (d) 100 torr x=1.7% (#17). The corresponding high magnification images are shown in (e)-(h).

Fig 8. Surface view FESEM images of low-Al β-(Al_xGa_{1-x})₂O₃ (x=~2%) films grown with different film thickness: (a) 5.5 μm (#7), (b) 11 μm (#11), and (c) 16.5 μm (#16). The corresponding AFM images (5μm x 5μm scan area) of low-Al β-(Al_xGa_{1-x})₂O₃ films with: (d) 5.5 μm (#7), (e) 11 μm (#11), and (f) 16.5 μm (#16).

Table 1

Sample ID	TMGa molar flow rate (µmol/min)	TMAI molar flow rate (μmol/min)	AI/(AI+Ga) (gas flow ratio)	Al composition (from XRD)	Silane molar flow rate (nmol/min)	Chamber pressure (torr)	Film thickness (um)	Growth rate (um/h)
#1	58	0	0	0	0.248	60	3	3
#2	58	0.46	0.79%	0.70%	0.248	60	3	3
#3	58	0.92	1.60%	1.30%	0.68	60	3	3
#4	58	1.78	3%	2.70%	0.68	60	3	3
#5	87	0	0	0	5.45	60	5.5	5.5
#6	87	2.21	2.50%	1.70%	5.45	60	5.5	5.5
#7	87	2.76	3%	2.00%	5.45	60	5.5	5.5
#8	87	3.43	3.80%	2.55%	5.45	60	5.5	5.5
#9	87	3.17	3.50%	2.20%	5.84	60	11	5.5
#10	87	3.03	3.37%	2.10%	5.84	60	11	5.5
#11	87	2.76	3.10%	1.90%	5.84	60	11	5.5
#12	87	2.35	2.60%	1.70%	5.84	60	11	5.5
#13	87	1.93	2.20%	1.30%	5.84	60	11	5.5
#14	87	1.5	1.70%	1.10%	5.84	60	11	5.5
#15	87	0	0	0	5.84	60	11	5.5
#16	87	2.76	3.10%	1.90%	21.84	60	16.5	5.5
#17	87	2.76	3.10%	1.70%	5.84	100	10.9	3
#18	87	2.76	3.10%	1.80%	5.84	80	11.2	4.25
#19	87	2.76	3.10%	2.17%	5.84	40	10.2	6.13

Table 2

Sample ID	TMGa molar flow rate (μmol/min)	TMAI molar flow rate (μmol/min)	AI/(AI+Ga) (gas flow ratio)	Al composition (from XRD)	Silane molar flow rate (nmol/min)	Chamber pressure (torr)	Film thickness (um)	Growth rate (um/h)	Electron concentration (cm ⁻³)	Hall mobility (cm²/Vs)
#1	58	0	0	0	0.248	60	3	3	6.31 x10 ¹⁶	171
#2	58	0.46	0.79%	0.70%	0.248	60	3	3	6.28 x10 ¹⁶	161
#3	58	0.92	1.60%	1.30%	0.68	60	3	3	1.43 x10 ¹⁷	144
#4	58	1.78	3%	2.70%	0.68	60	3	3	1.38 x10 ¹⁷	132
#6	87	2.21	2.50%	1.70%	5.45	60	5.5	5.5	5.14 x10 ¹⁷	113
#7	87	2.76	3%	2.00%	5.45	60	5.5	5.5	4.45 x10 ¹⁷	104
#8	87	3.43	3.80%	2.55%	5.45	60	5.5	5.5	4.23 x10 ¹⁷	70

Figure 1

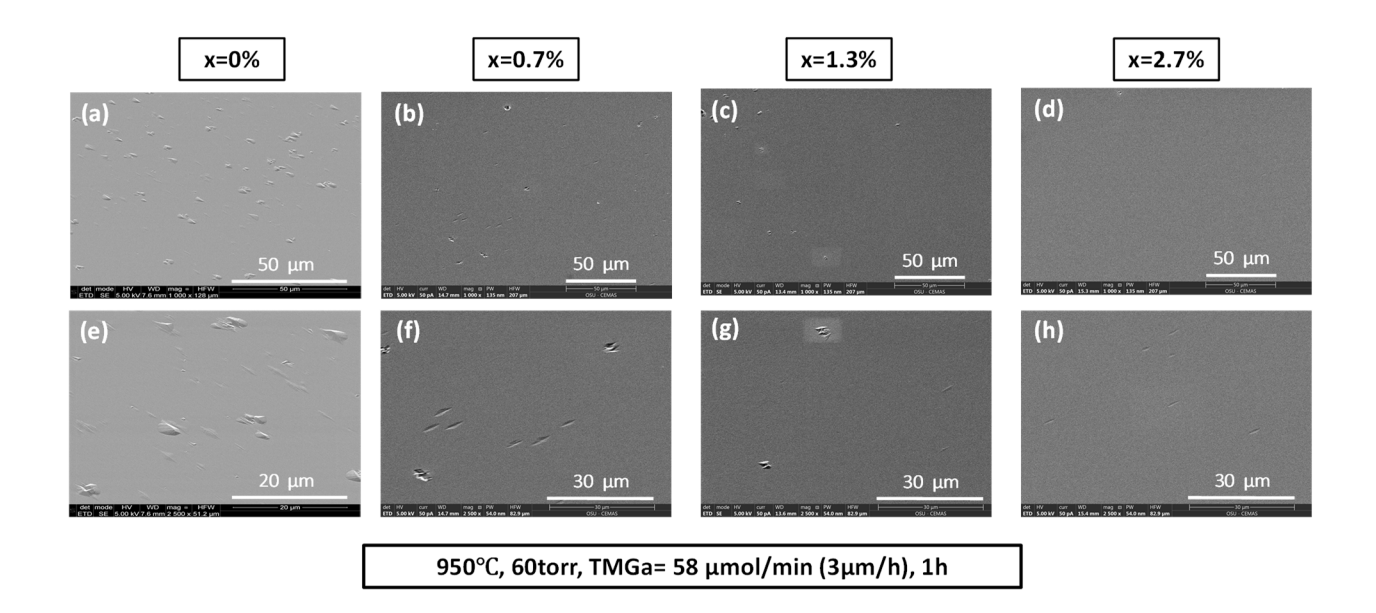


Figure 2

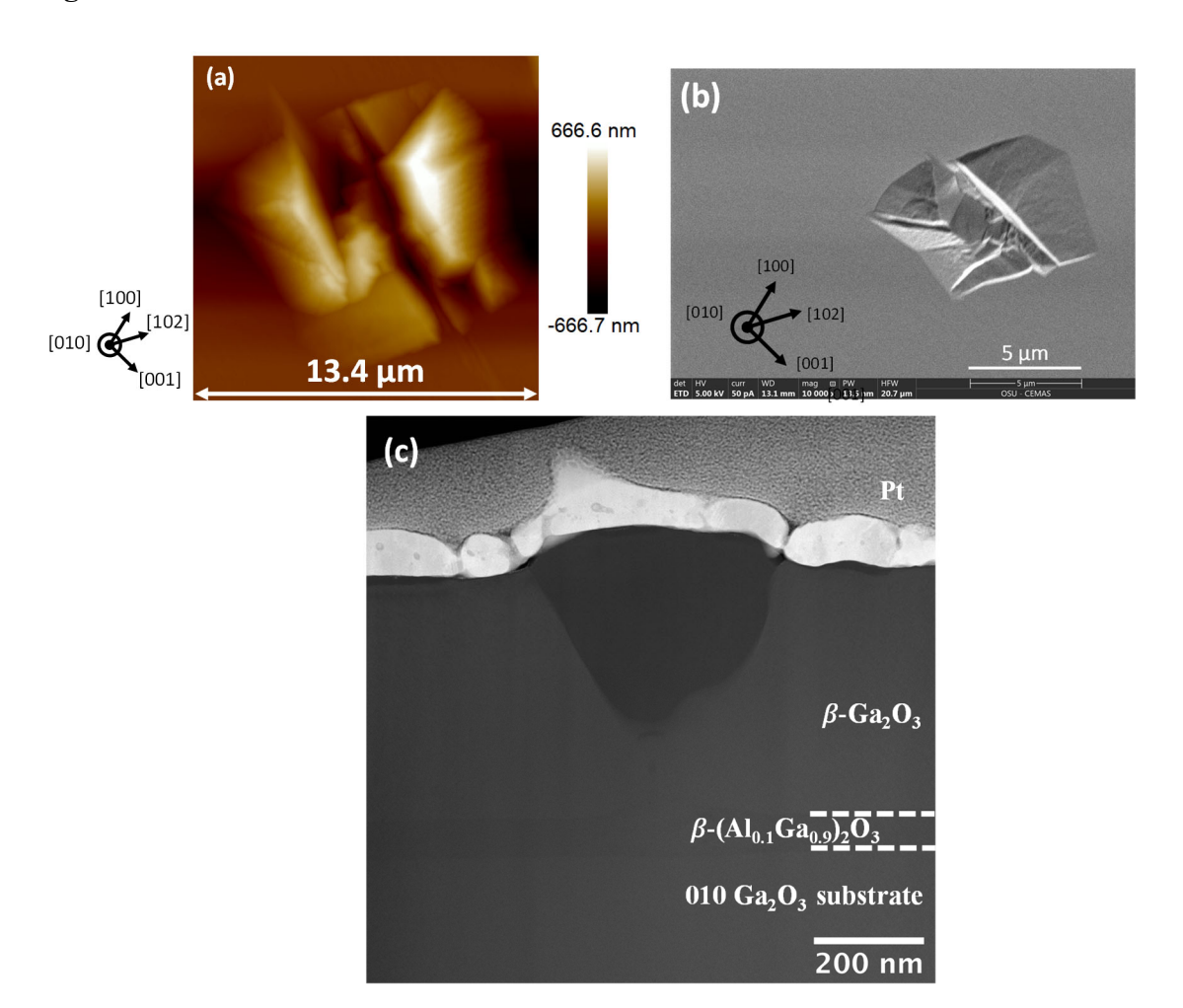


Figure 3

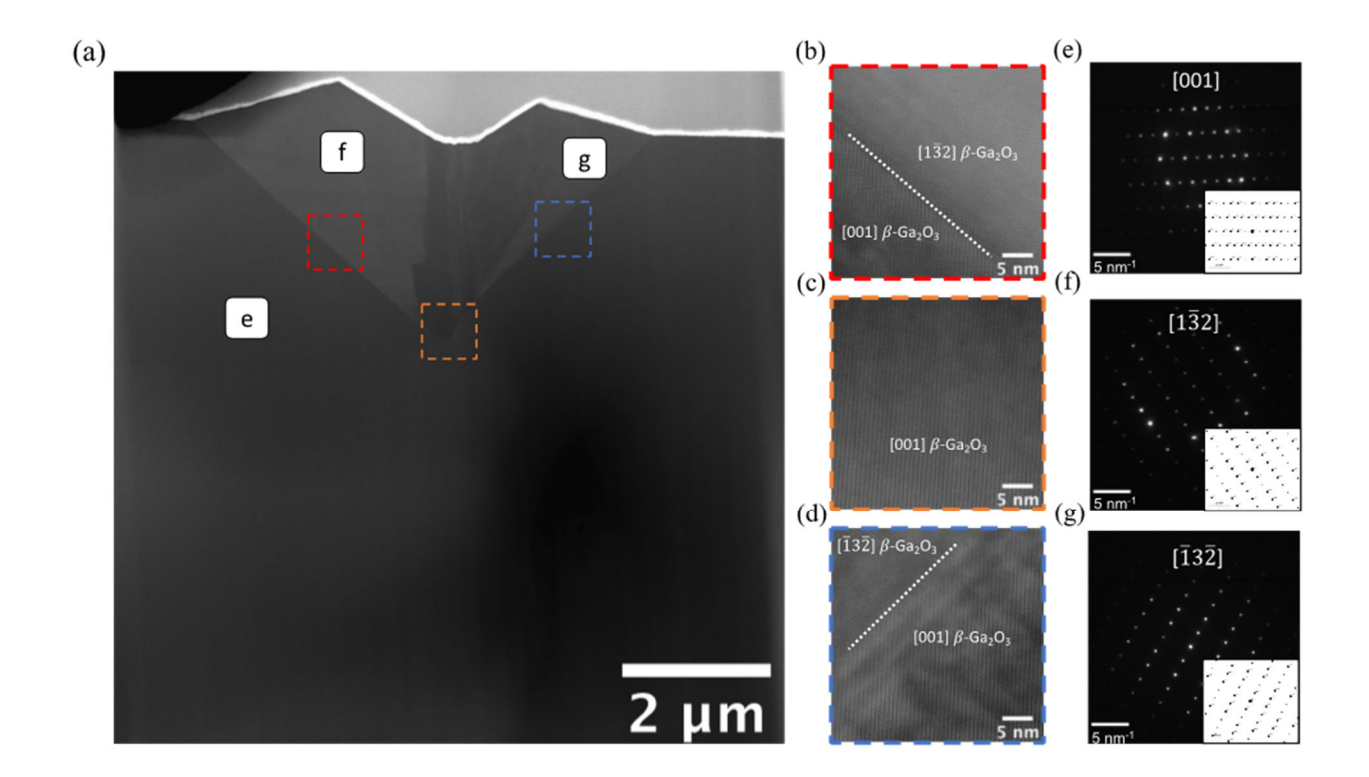


Figure 4

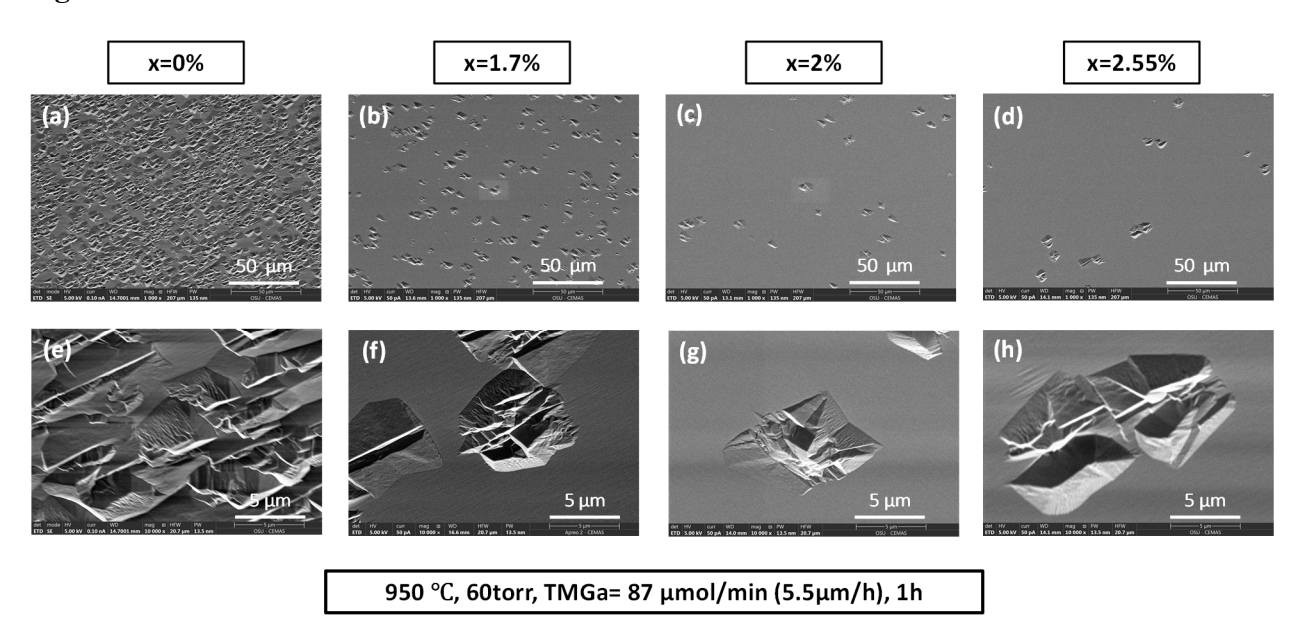


Figure 5

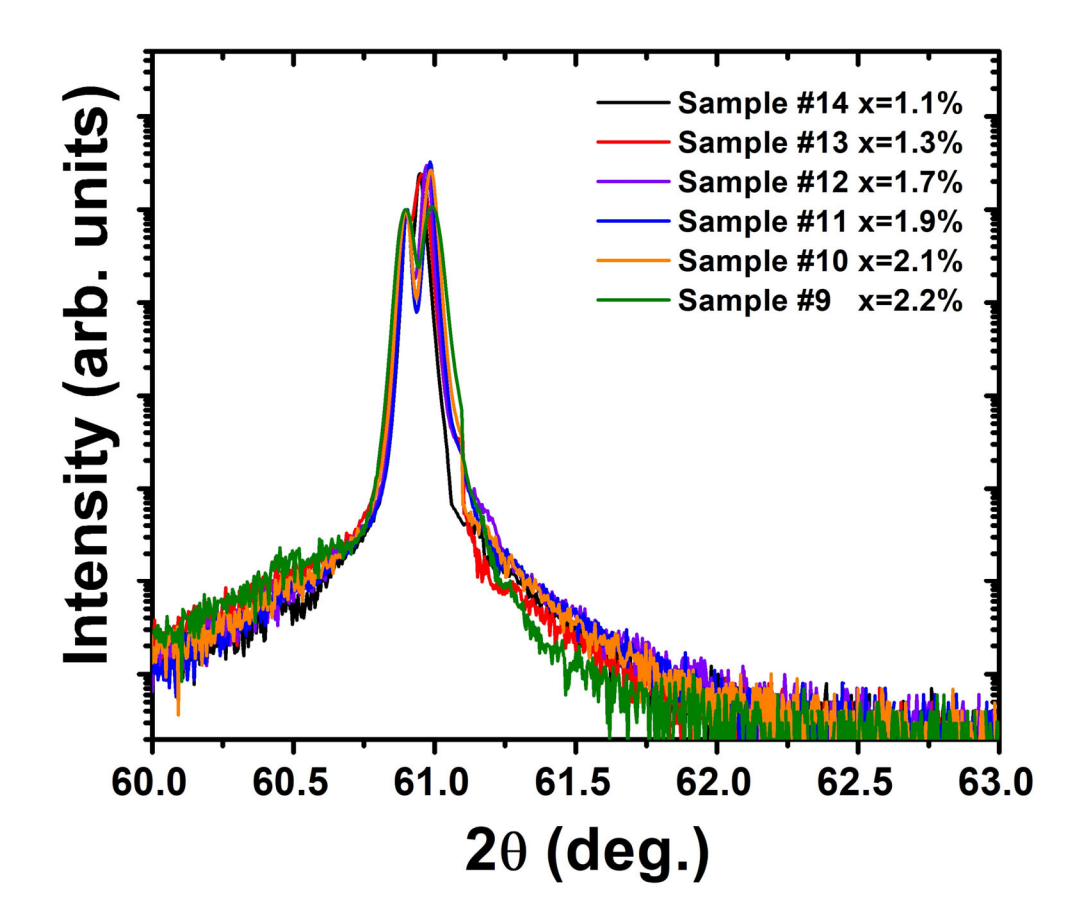


Figure 6

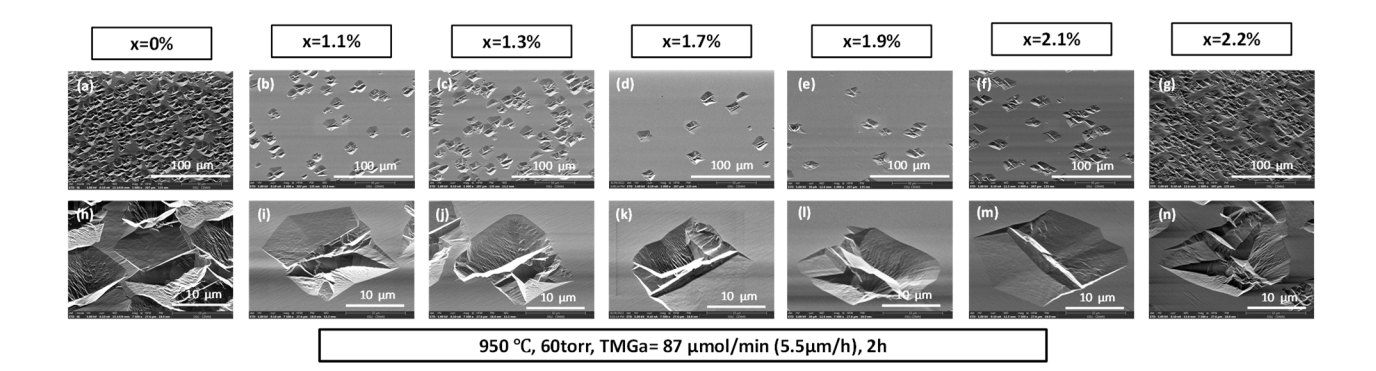
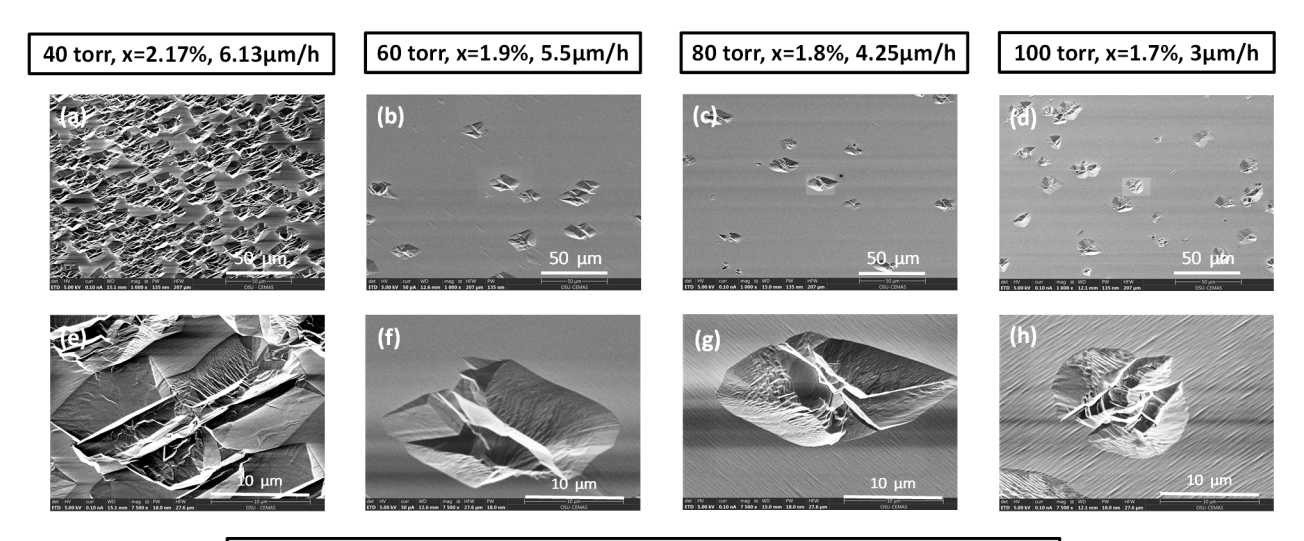
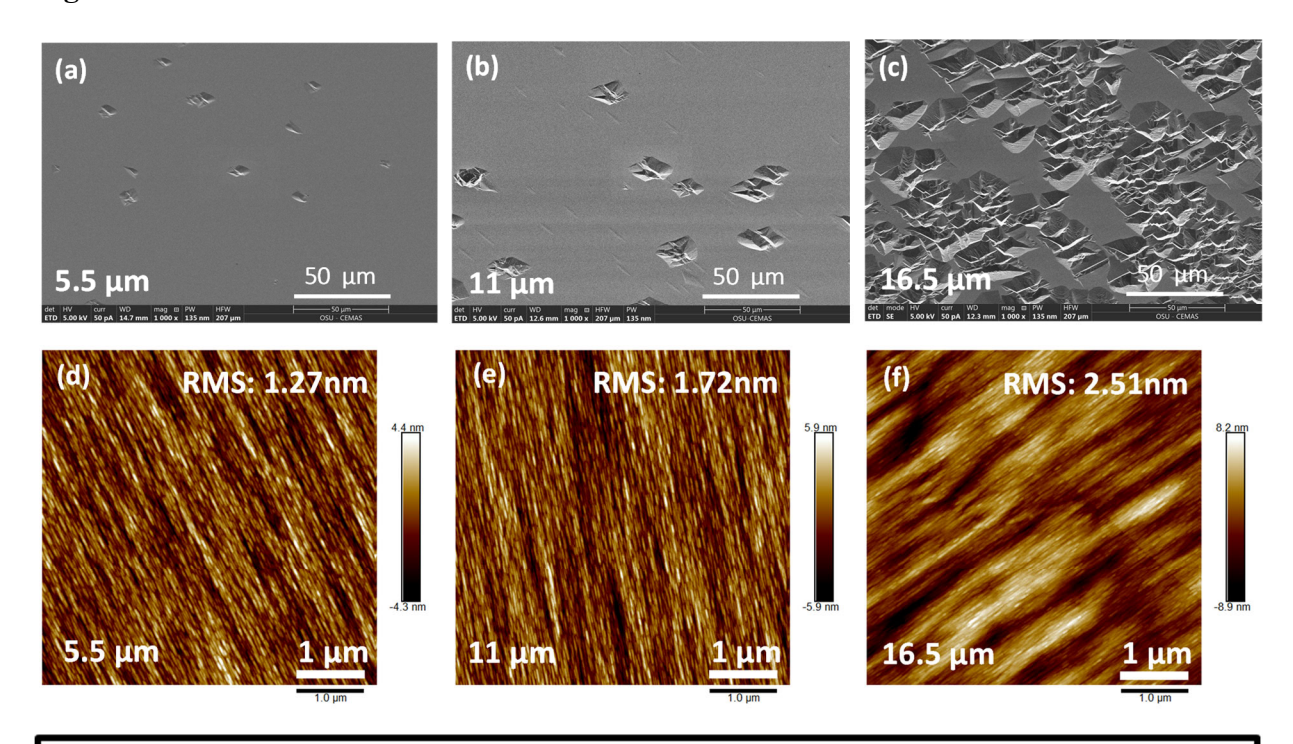


Figure 7



950 °C, Al/(Al+Ga)=3.1%, TMGa= 87 μ mol/min, film thickness=~11um

Figure 8



950 °C, 60torr, TMGa= 87 μmol/min (5.5μm/h), Al=~2%

For Table of Contents Use Only

MOCVD growth of thick β-(Al)GaO films with fast growth rates

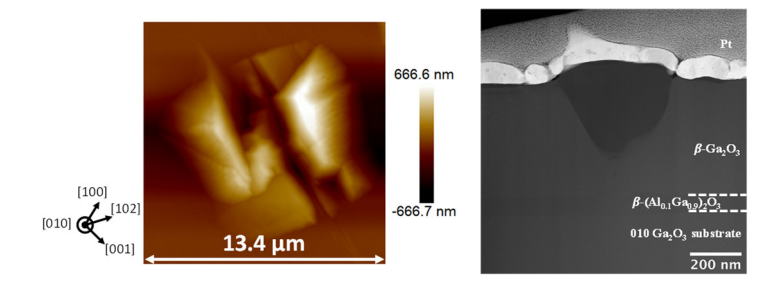
Lingyu Meng^{1,*}, A F M Anhar Uddin Bhuiyan¹, Dongsu Yu¹, Hsien-Lien Huang², Jinwoo Hwang², and Hongping Zhao^{1,2,‡}

¹Department of Electrical and Computer Engineering, The Ohio State University, Columbus, OH 43210, USA

²Department of Materials Science and Engineering, The Ohio State University, Columbus, OH 43210, USA

*Email: meng.480@osu.edu

‡Corresponding Author Email: zhao.2592@osu.edu



Pyramid-shaped defects were identified in (010) β -Ga₂O₃ films grown via MOCVD with trimethylgallium as the precursor and at relatively fast growth rates. Incorporation of low-Al composition was demonstrated to significantly improve film quality and surface morphology. We achieved the best surface for β -(Al_xGa_{1-x})₂O₃ in an 11 μ m-thick film with ~2% Al composition, grown at a rate of 5.5 μ m/h.